Hindawi Publishing Corporation
Journal of Nanomaterials
Volume 2012, Article ID 163909, 8 pages
doi:10.1155/2012/163909

Research Article

Formation of Nanoscale $Mg_{(x)}Fe_{(1-x)}O$ $(x = 0.1, 0.2, 0.4)$ Structure by Solution Combustion: Effect of Fuel to Oxidizer Ratio

Mohsen Ahmadipour, K. Venkateswara Rao, and V. Rajendar

Center for Nanoscience and Technology, Institute of Science and Technology, Jawaharlal Nehru Technological University Hyderabad, Hyderabad 500085, India

Correspondence should be addressed to K. Venkateswara Rao, kalagadda2003@yahoo.com

Received 25 July 2012; Accepted 10 October 2012

Academic Editor: Miguel A. Correa-Duarte

$Mg_{(x)}Fe_{(1-x)}O$ (magnesiowustite) nanopowder samples synthesized by solution-combustion method and fuel to oxidizer ratio ($\Psi = 1, 1.25$) are used as a control parameter to investigate how particle size and morphology vary with Ψ. The method is inexpensive and efficient for synthesis of oxide nanoparticles. The average crystallite size of $Mg_{(x)}Fe_{(1-x)}O$ nanoparticles was estimated from the full-width-half maximum of the X-ray diffraction peaks of powders using Debye-Scherrer's formula; the average crystallite size varies from 16 nm to 51 nm. From X-ray diffraction analysis, it was observed that $Mg_{(x)}Fe_{(1-x)}O$ nanoparticles have cubic structure. The particle size measured by particle size analyzer ranges from 37.7 nm to 73 nm which is in the order of XRD results. Thermal analysis was done by thermal gravimetric-differential thermal analyzer. The particle size and morphology of the synthesized powder were examined by transmission electron microscope and scanning electron microscope. The crystal size and particle size were compared with some of the most recently published research works by XRD and TEM. FTIR conforms formation of the $Mg_{(x)}Fe_{(1-x)}O$.

1. Introduction

Magnetic Nanoparticles (NPs) have many unique magnetic properties such as super paramagnetic, high coactivity, low Curie temperature, high magnetic susceptibility, and so forth. Magnetic NPs are of great interest for researchers from a broad range of disciplines [1–5], microwaves devices, magnetic recording media, fabrication of radio frequency coils, transformer cores, chock coils, noise filters, and recording, heading, and rod antennas [6–8] and also are very important in heterogeneous catalysis, adsorption, and sensors [9, 10]. Especially, magnetic Ferro fluids and data storage are the applied researches that have led to the integration of magnetic NPs in a myriad of commercial applications.

In recent years, various physical and chemical techniques such as sol-gel [11], coprecipitation method [12, 13], microwave hydrothermal method [14], micro emulsion method [15], electrospinning [16], and ball milling [17] have been successfully employed for the synthesis of $Mg_{(x)}Fe_{(1-x)}O$ nanoparticles.

In the present work, Solution Combustion Synthesis technique (SCS) has been used and is known as one of the effective and economic method [18]. Solution Combustion synthesis (CS) [19] has emerged as an important technique for the synthesis and processing of advanced ceramics (structural and functional), catalysts, composites, alloys, and intermetallic and nanomaterial. The method exploits self-sustaining solid flame combustion reaction for the internal development of very short period [20]. Fuel to oxidizer ratio [21] is very crucial and effective amount in this method [22], it can change the properties of the Nanomaterial as the reaction temperature depends on fuel to oxidizer ratio. It is well recognized that the fuel is an important component for the preparation of oxides by SCS. However, there are not many studies that have been found in the literature correlating the microstructure and effect of grain size with the magnetic properties of $Mg_{(x)}Fe_{(1-x)}O$ powders.

2. Experimental

The $Mg_{(x)}Fe_{(1-x)}O$ powders were prepared by using combustion synthesis in solution under different molar compositions of fuel (glycine, NH_2CH_2COOH) and fuel to oxidizer ratio $\Psi = 1$ and $\Psi = 1.25$. The iron nitrate ($Fe(NO_3)_3 \cdot 9H_2O$) and magnesium nitrate ($Mg(NO_3)_3 \cdot 6H_2O$) were dissolved in a beaker with sufficient deionized water with glycine in appropriate amount and the solution was placed under thermal stirring with the temperature of 60°C; at this temperature, different molar amounts of the fuel were added. The precursor solutions were maintained under thermal stirring for few minutes to ensure homogeneity, subsequently these solutions were placed in a hot plate. As the temperature reached 100°C, water started to boil and evaporate from the solution which increased solution viscosity substantially. The obtained precursor is annealed for 2 h at 300°C. The decomposition reactions of starting compositions are

$$Mg(No_3)_2 \cdot 6H_2O \longrightarrow MgO + NO_2 + 6H_2O \quad (1)$$

$$Fe(NO_3)_3 \cdot 9H_2O \longrightarrow \frac{1}{3}Fe_3O_4 + \frac{3}{2}NO + \frac{3}{2}NO_2 + 16O_2 + 9H_2O \quad (2)$$

$$NH_2CH_2COOH + \frac{9}{2}O_2 \longrightarrow N_2 \uparrow + 4CO_2 \uparrow + 5H_2O \uparrow \quad (3)$$

The overall combustion reaction in air may be written as

$$X Mg(NO_3)_2 \cdot 6H_2O + (1-X)Fe(NO_3)_3 \cdot 9H_2O + NH_2CH_2COOH \longrightarrow Mg_{(x)}Fe_{(1-x)}O + CO_2 \uparrow + N_2 \uparrow + H_2O \uparrow \quad (4)$$

The crystal phase of the synthesized powders were determined by X-ray diffraction (XRD, Bruker D8 Advance, Germany) using Cu Kα as radiation source (40 kV, step size 0.02, scan rate 0.5 min^{-1}). The particle sizes were measured by nanoparticle size analyzer (SZ-100 Nanoparticle, Horiba, Japan). The thermal decomposition behaviors of the precursors were investigated by thermogravimetric analysis (TGA/DTA, SII EXSTAR 6300R, Japan). Fourier transform infrared spectroscopy was used as well (FTIR, PERKIN ELMER, India). The particles size and morphology of the synthesized powder were examined by scanning electron microscope (SEM, S-3400N-hitachi-Japan), transmission electron microscope (TEM, JEM-2100, Jeol).

3. Result and Discussion

3.1. Crystal Analysis. The crystalline phases present in the different samples were identified by X-ray diffraction (XRD) on a Bruker axis D8 diffractometer using Cu-Kα (λ = 1.5406 Å) radiation and secondary monochromator in the range 2θ from 20°C to 80°C. The crystallite size of magnesiwuestite present was investigated based on X-ray diffraction

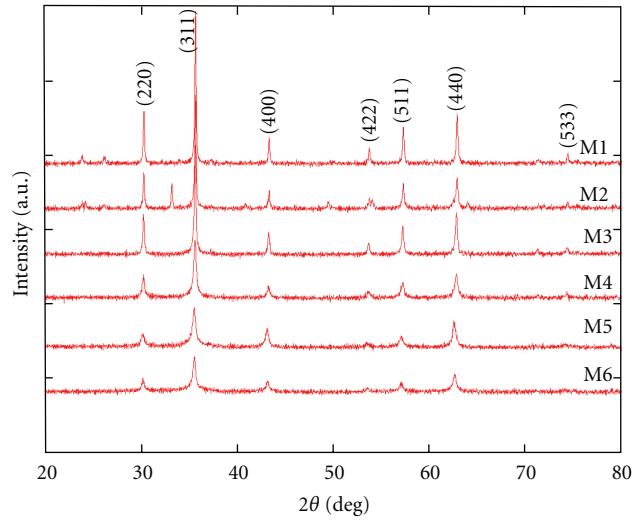

Figure 1: Room temperature XRD patterns of $Mg_{(x)}Fe_{(1-x)}O$ nanoparticles prepared by solution combustion with different fuel to oxidizer ratios (Ψ) at 300°C, (M1) $\Psi = 1$, (M2) $\Psi = 1.25$, (M3) $\Psi = 1$, (M4) $\Psi = 1.25$, (M5) $\Psi = 1$, and (M6) $\Psi = 1.25$.

line broadening and calculated by using full-width at half-maximum (FWHM) of the XRD all peaks by making use of the Debye-Scherrer formula [32], then the average was extracted

$$D = \frac{0.9\lambda}{\beta \cos\theta}, \quad (5)$$

where D is the crystallite size, λ is the wavelength of Cu-Kα radiation, θ is a diffraction angle, and β is full-width at half-maximum (FWHM) of the XRD all peaks. Figure 1 shows the XRD pattern of the synthesized nanopowder; the graphs show different Ψ values. It is clear cut that a spinel structure of magnesiwuestite which is described in (JCPDS 89–4924) is detected in all samples. Seven peaks centered at $2\theta = 30.28$°C, 35.66°C, 43.33°C, 53.77°C, 57.31°C, 62.93°C, and 74.44°C, which correspond to diffraction planes of (2 2 0), (3 1 1), (4 0 0), (4 2 2), (5 1 1), (4 4 0), and (5 3 3), respectively, are detected.

According to JCPDS 89–4924, the obtained phase has a cubic structure. The existence of a peak around the diffraction angle (2θ) equal to 35.66°C corresponding to (3 1 1) plane confirms the formation of spinel ferrites. A careful analysis of XRD patterns helps to determine their respective planes and face-centered cubic structure of these ferrites. Another method used to calculate particle size is Williamson-Hall equation [33]:

$$\beta \cos\theta = \frac{k\lambda}{D} + \beta\varepsilon \sin\theta, \quad (6)$$

where β is full-width at half-maximum (FWHM) of the XRD all peaks, λ is the wavelength of Cu-Kα radiation (constant), k is Scherrer constant, D is the crystallite size, ε is the micro strain, and θ is the Bragg angle. Using a linear line to this plot, the slope gives the strain and the intercept gives the particle size ($k\lambda/D$).

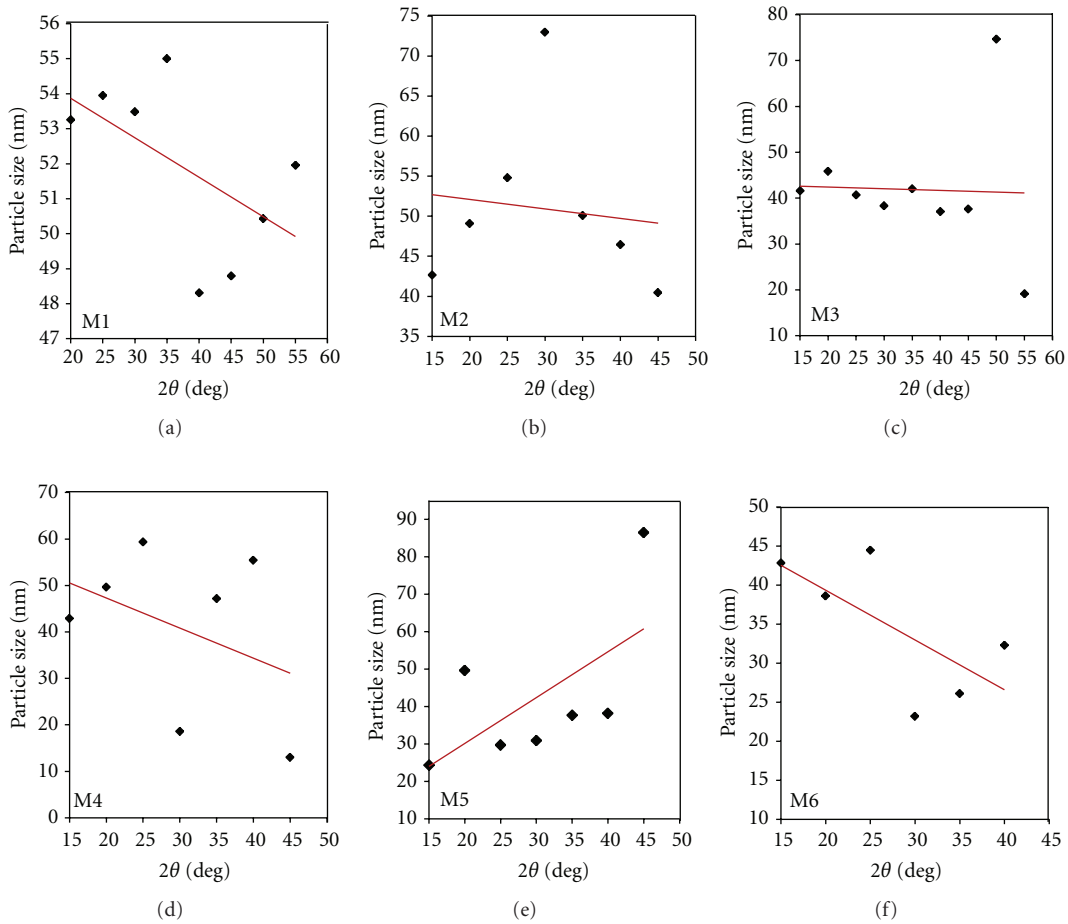

Figure 2: (a, b, c, d, e, f) Plots of peak position versus crystallite size (M1) $\Psi = 1$, (M2) $\Psi = 1.25$, (M3) $\Psi = 1$, (M4) $\Psi = 1.25$, (M5) $\Psi = 1$, and (M6) $\Psi = 1.25$, respectively.

Table 1: Crystalline size calculated from XRD, Williamson-Hall equation, and particle size analyzer (SZ-100).

Sample	Ψ	Williamson-Hall crystalline size (nm)	Debye-Scherrer crystalline size (nm)	Particle size analyzer
$Mg_{0.1}Fe_{0.9}O$	1	22 ± 059	51.95	73
$Mg_{0.1}Fe_{0.9}O$	1.25	18 ± 074	50.9	72.1
$Mg_{0.2}Fe_{0.8}O$	1	21 ± 46	34.4	70.9
$Mg_{0.2}Fe_{0.8}O$	1.25	21 ± 48	27.94	70.2
$Mg_{0.4}Fe_{0.6}O$	1	20 ± 60	24.42	43.7
$Mg_{0.4}Fe_{0.6}O$	1.25	21 ± 066	16.45	37.7

Based on the diffraction peak positioned at different degrees, the crystallite size is estimated by plotting crystallite size versus peak positions and extrapolation of the straight line by linearly fitting the points (Figure 2).

Table 1 Shows crystallite size (D) (nm) with Williamson-Hall equation, XRD, and particle size analyzer (SZ-100). Particle size of $Mg_{(x)}Fe_{(1-x)}O$ is done by particle size analyzer (SZ-100). Small amount of sample is dissolved in ethanol then sonicated to form clear solution. The particle sizes which were estimated by particle size analyzer (SZ-100) are greater than the particle sizes which were estimated by XRD with Dybe-Scherrer's formula.

3.2. Thermal Analysis. Figure 3 illustrates the thermogravimetric curve of the $Mg_{(x)}Fe_{(1-x)}O$ powder precursor after calcination at 300°C. Thermal analysis of $Mg_{(x)}Fe_{(1-x)}O$ samples was carried out in air atmosphere. It is well known that materials with a cubic crystal structure are prone to grow into a spherical shape [34–36] to minimize the surface tension. Thermogravimetric method measures the mass of a sample as the temperature increasing. This method is useful for determining sample purity of water, carbonate, and organic content and for studying decomposition reaction. TG curve shows consistent weight loss as it is illustrated in Figure 3. Among the samples which are placed in

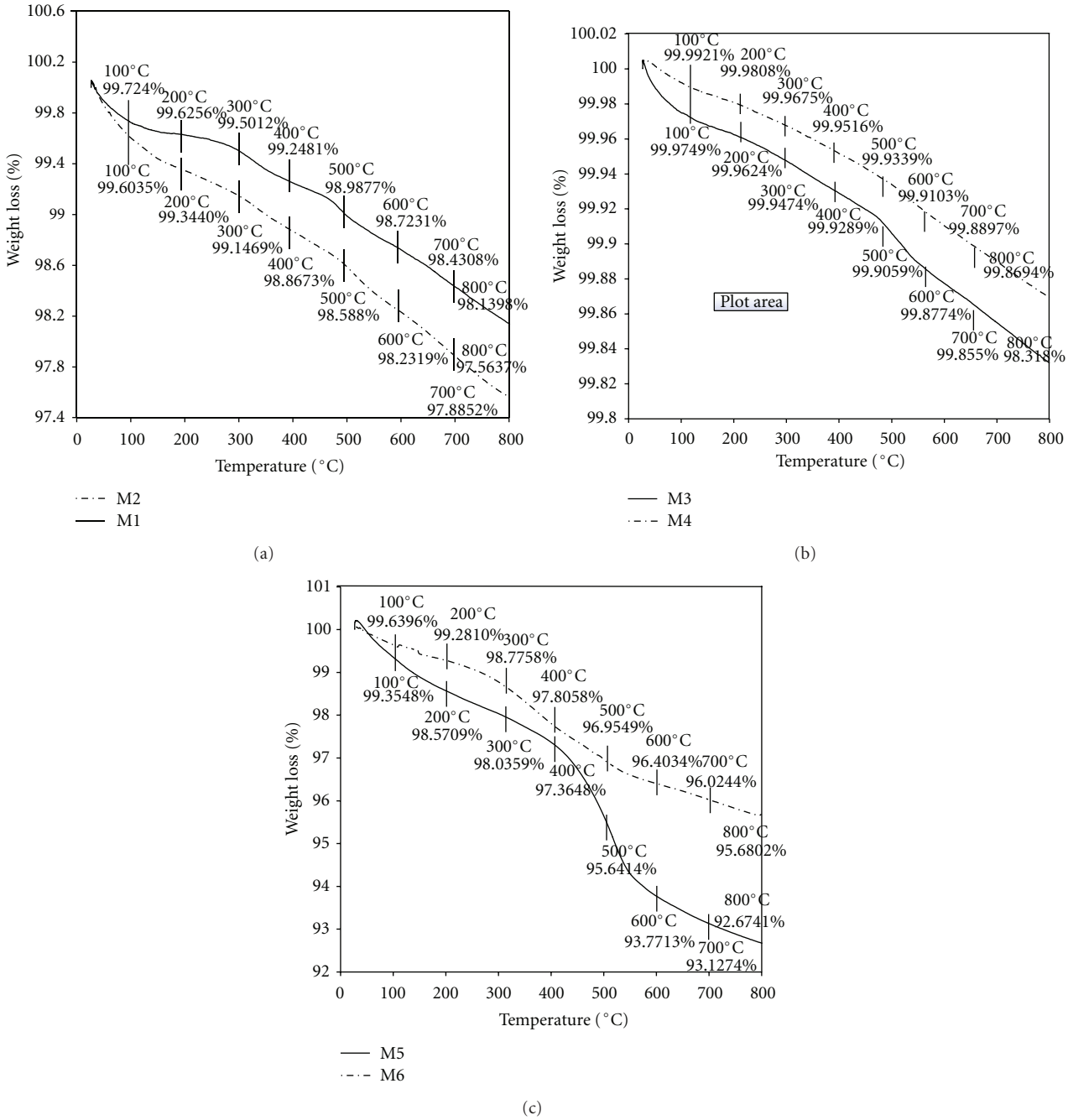

Figure 3: (a, b, c) TGA curve for nano crystalline $Mg_{(x)}Fe_{(1-x)}O$ for (M1) $\Psi = 1$, (M2) $\Psi = 1.25$, (M3) $\Psi = 1$, (M4) $\Psi = 1.25$, (M5) $\Psi = 1$, and (M6) $\Psi = 1.25$, respectively.

TG-DTA after calcination, less weight loss and impurity were observed. The net weight loss is illustrated in Table 2.

3.3. Fourier Transform Infrared Spectroscopy Analysis. The FTIR spectra measurement of fresh $Mg_{(x)}Fe_{(1-x)}O$ Nanoparticles in the range of 4000–450 cm^{-1} are shown in Figure 4. A broad absorption spectrum is seen around 3430 cm^{-1} which is a characteristic stretching vibration of hydroxylate group (O–H). Peaks localized at 1560 cm^{-1} and 1411 cm^{-1} are assigned to asymmetrical and symmetrical stretching vibration of carboxylate (O–C–O), respectively.

IR spectrum of magnesiwuestite is found to exhibit two major bands in the range of 450–700 cm^{-1}. The bands in the region 450 to 700 cm^{-1} are attributed to the fundamental vibrations of the ions of the crystal lattice. For the analysis of such spectra, it is necessary to consider the vibrational spectrum of periodic structures. The 1400 cm^{-1} (broad) characterizes the formation of surface sulfate species with S=O bond. The high frequency band is around 1561 cm^{-1}.

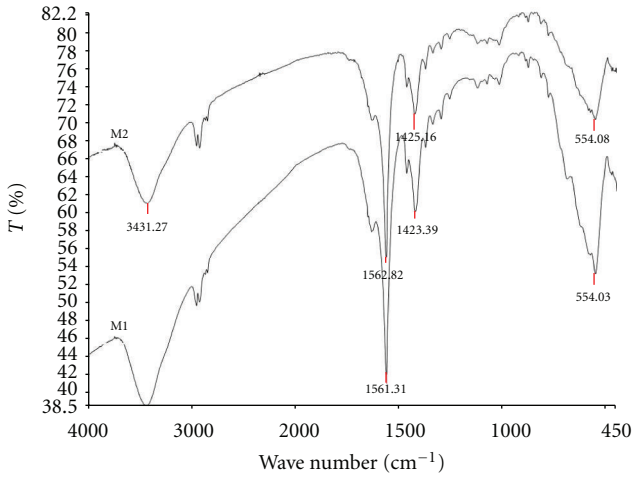

Figure 4: FT-IR spectra of the $Mg_{(x)}Fe_{(1-x)}O$ powders produced by combustion method at 300°C with different fuel to oxidizer ratios (Ψ).

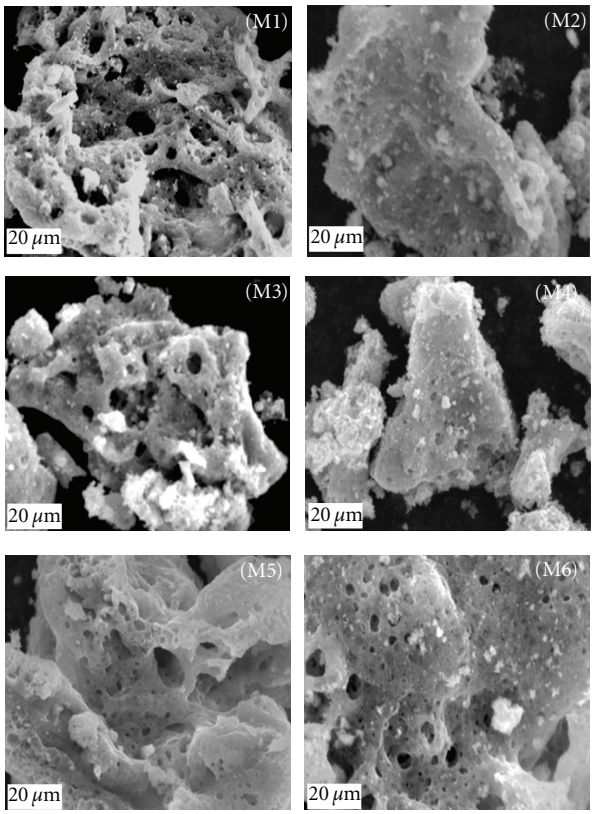

Figure 5: SEM micrograph of sample, scale bar 20 μm, (M1) $\Psi = 1$, (M2) $\Psi = 1.25$, (M3) $\Psi = 1$, (M4) $\Psi = 1.25$, (M5) $\Psi = 1$, (M6) $\Psi = 1.25$ calcined in air for 2 h at 300°C.

This band is a common feature to all the ferrites [37]. Absorption bands due to the iron-oxygen (Fe–O) are observed in the range 450–550 cm^{-1}. The other peaks are due to the presence of magnesiwuestite. Same peaks are observed for all samples.

3.4. Morphology. Figures 5–7 show the detailed morphology and crystalline structure of the $Mg_{(x)}Fe_{(1-x)}O$ nanopowder which is calcined at 300°C for 2 h, then further investigated by SEM, TEM, and selected-area electron diffraction (SAED). TEM can be used to measure the particle size of individual particles, which is one of the most basic parameters in nanoparticle research. Transmission electron microscopy (TEM) shows the particle's morphology, distribution, and size. The particle size estimated from TEM is smaller than the crystallite size estimated from XRD using

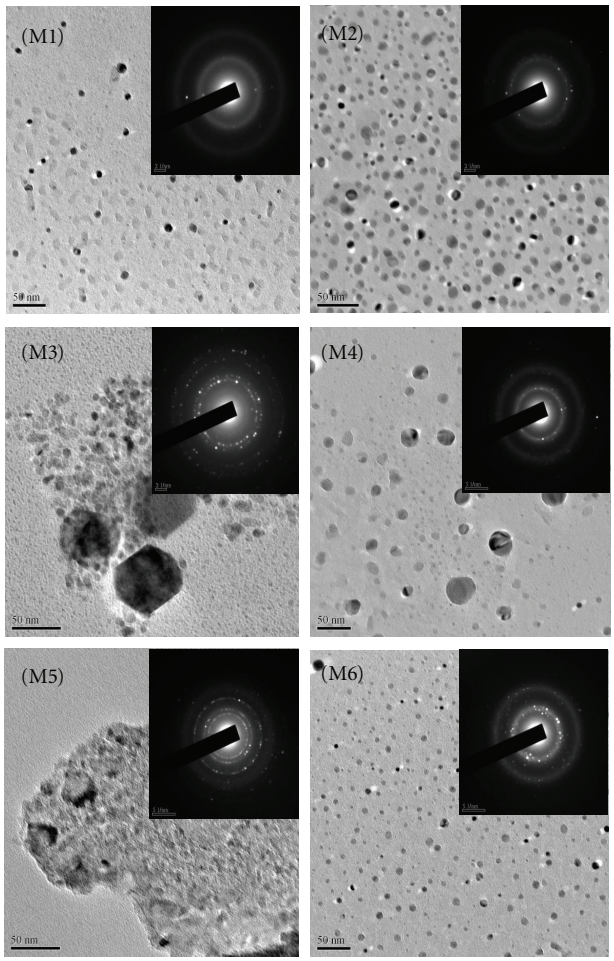

Figure 6: TEM image with corresponding SAED patterns of the samples, scale bar 50 nm, (M1) $\Psi = 1$, (M2) $\Psi = 1.25$, (M3) $\Psi = 1$, (M4) $\Psi = 1.25$, (M5) $\Psi = 1$, and (M6) $\Psi = 1.25$ calcined in air for 2 h at 300°C.

Table 2: Net weight loss illustration.

Sample	x	Formula	Start, end point (%)	Net weight loss (%)
M1	0.1	$Mg_{0.1}Fe_{0.9}O$	100–98.12	1.87
M2	0.1	$Mg_{0.1}Fe_{0.9}O$	100–97.55	2.44
M3	0.2	$Mg_{0.2}Fe_{0.8}O$	100–99.83	0.16
M4	0.2	$Mg_{0.2}Fe_{0.8}O$	100–99.86	0.13
M5	0.4	$Mg_{0.4}Fe_{0.6}O$	100–99.78	0.21
M6	0.4	$Mg_{0.4}Fe_{0.6}O$	100–95.62	4.37

Dybe-Scherer's formula. The same is perceived from EDS graph for six samples and EDS also shows the percentage of element in the powders. It can be seen in Figure 6 that the particles are quite well dispersed and not much agglomerations are present. The percentage of element is shown in the EDS table. Comparison table for crystallite and particle size from XRD and TEM characterizations of present and previous papers are given in Table 3.

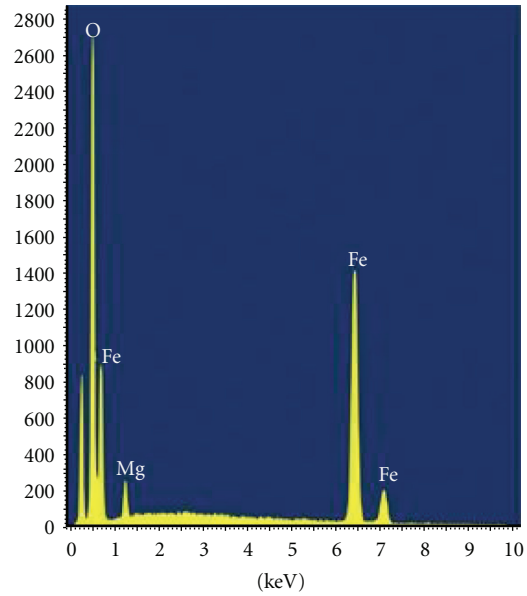

Element	Percentage
O	52.5
Mg	4.77
Fe	42.74
Total	100

Figure 7: EDS of sample calcined at 300°C for 2 hr. (M1) $\Psi = 1$, (M2) $\Psi = 1.25$, (M3) $\Psi = 1$, (M4) $\Psi = 1.25$, (M5) $\Psi = 1$, and (M6) $\Psi = 1.25$ and also indicated table for EDS pattern is shown in right side.

$Mg_{(x)}Fe_{(1-x)}O$ was observed to have high porous structure which was shown in Figure 5.

4. Conclusion

The nanostructured $Mg_{(x)}Fe_{(1-x)}O$ powder samples were synthesized by simple eco-friendly solution-combustion with economically and environmentally beneficial method. The average crystallite size of $Mg_{(x)}Fe_{(1-x)}O$ nanoparticles was estimated from the full-width-half maximum of the X-ray diffraction peaks and particle size analyzer and the results are in the same order. It was observed from XRD pattern that $Mg_{(x)}Fe_{(1-x)}O$ nanoparticles have cubic structure. Thermal analysis was done by Thermogravimetric-Differential thermal analyzer which shows weight loss percentage. FTIR conforms formation of the $Mg_{(x)}Fe_{(1-x)}O$. The results reported in this study could be applied for establishing a simple method for the preparation of $Mg_{(x)}Fe_{(1-x)}O$ nanopowders. The synthesis process is economically and environmentally beneficial, inexpensive, and efficient method when compared to other solid state reactions. It was observed that $Mg_{(x)}Fe_{(1-x)}O$ has porous structure as it is shown in Figure 5 and has finer dispersion with spherical morphology of particles as illustrated in Figure 6.

Table 3: Comparison of particle size determined from TEM.

Methods	Particle size (TEM) (nm)	Crystal size (XRD) (nm)	References
(i) Air oxidation	Not mentioned	26	[23]
(ii) Ball milling	50	Not mentioned	[24]
(iii) Combustion reaction	20–30	18–61	[25]
(iv) Combustion route	10–20 and 25–80	$16 \pm 4, 18 \pm 1, 25 \pm 2, 26 \pm 3$	[26]
(v) Solid state reaction	10	15–30	[27]
(vi) Autocombustion assisted	7–8	7.4	[28]
(vii) Sol-gel method	Not mentioned	35	[29]
(viii) Combustion reaction	28–46	28–46	[30]
(ix) Microwave hydrothermal method	2	3	[31]
(x) Solution combustion synthesis	Figure 6	51.9, 50.9, 34.4, 27.9, 24.4, 16.4	Present works

Acknowledgments

The authors would like to thank the School of Engineering Sciences and Technology, Hyderabad University for providing XRD, EDS, SEM, Regional Sophisticated Instrumentation Centre for TEM, Mr. Masoud Ahmadipour, Department of Electrical and Computer Science, Semnan University, and Iran for cooperation and special thanks to K. V. Rao, Head of Center of Nano Science and Technology, Jawaharlal Nehru Technological University Hyderabad.

References

[1] D. Patel, J. Y. Moon, Y. Chang, T. J. Kim, and G. H. Lee, "Poly(d,l-lactide-co-glycolide) coated superparamagnetic iron oxide nanoparticles: synthesis, characterization and in vivo study as MRI contrast agent," *Colloids and Surfaces A*, vol. 313-314, pp. 91–94, 2008.

[2] M. Zhao, L. Josephson, Y. Tang, and R. Weissleder, "Angew magnetic sensors for protease assays," *Cheme International*, vol. 42, no. 12, pp. 1375–1378, 2003.

[3] S. Mornet, S. Vasseur, F. Grasset et al., "Magnetic nanoparticle design for medical applications," *Progress in Solid State Chemistry*, vol. 34, no. 2–4, pp. 237–247, 2006.

[4] P. D. Stevens, J. Fan, H. M. R. Gardimalla, M. Yen, and Y. Gao, "Superparamagnetic nanoparticle-supported catalysis of Suzuki cross-coupling reactions," *Organic Letters*, vol. 7, no. 11, pp. 2085–2088, 2005.

[5] Y. Jun, J. Choi, and J. Cheon, "Heterostructured magnetic nanoparticles: their versatility and high performance capabilities," *Chemical Communications*, no. 12, pp. 1203–1214, 2007.

[6] V. Šepelák, D. Baabe, D. Mienert et al., "Evolution of structure and magnetic properties with annealing temperature in nanoscale high-energy-milled nickel ferrite," *Journal of Magnetism and Magnetic Materials*, vol. 257, no. 2-3, pp. 377–386, 2003.

[7] M. Pavlovic, C. Jovalekic, A. S. Nikolic, D. Manojlovic, and N. Sojic, "Mechanochemical synthesis of stoichiometric $MgFe_2O_4$ spinel," *Journal of Materials Science*, vol. 20, no. 8, pp. 782–787, 2009.

[8] P. Holec, J. Plocek, D. Nižňanský, and J. Poltierová Vejpravová, "Preparation of $MgFe_2O_4$ nanoparticles by microemulsion method and their characterization," *Journal of Sol-Gel Science and Technology*, vol. 51, no. 3, pp. 301–305, 2009.

[9] M. Tada, T. Kanemaru, T. Hara, T. Nakagawa, H. Handa, and M. Abe, "Synthesis of hollow ferrite nanospheres for biomedical applications," *Journal of Magnetism and Magnetic Materials*, vol. 321, no. 10, pp. 1414–1416, 2009.

[10] G. Zhang, C. Li, F. Cheng, and J. Chen, "$MgFe_2O_4$ tubes: synthesis and application to gas sensors with high sensitivity and low-energy consumption," *Sensors and Actuators, B*, vol. 120, no. 2, pp. 403–410, 2007.

[11] L. J. Berchmans, R. K. Selvan, P. N. S. Kumar, and C. O. Augustin, "Structural and electrical properties of $Ni_{1-x}Mg_xFe_2O_4$synthesized by citrate gel process," *Journal of Magnetism and Magnetic Materials*, vol. 279, no. 1, pp. 103–110, 2004.

[12] C. P. Liu, M. W. Li, Z. Cui et al., "Comparative study of magnesium ferrite nanocrystallites prepared by sol-gel and coprecipitation methods," *Journal of Materials Science*, vol. 42, no. 15, pp. 6133–6138, 2007.

[13] Q. Chen, A. J. Rondinone, B. C. Chakoumakos, and Z. J. Zhang, "Synthesis of superparamagnetic $MgFe_2O_4$ nanoparticles by coprecipitation," *Journal of Magnetism and Magnetic Materials*, vol. 194, no. 1–3, pp. 1–7, 1999.

[14] S. Verma, P. A. Joy, Y. B. Khollam, H. S. Potdar, and S. B. Deshpande, "Synthesis of nanosized $MgFe_2O_4$ powders by microwave hydrothermal method," *Materials Letters*, vol. 58, no. 6, pp. 1092–1095, 2004.

[15] P. Holec, J. Plocek, D. Nižňanský, and J. Poltierová Vejpravová, "Preparation of $MgFe_2O_4$ nanoparticles by microemulsion method and their characterization," *Journal of Sol-Gel Science and Technology*, vol. 51, no. 3, pp. 301–305, 2009.

[16] S. Maensiri, M. Sangmanee, and A. Wiengmoon, "Magnesium ferrite ($MgFe_2O_4$) nanostructures fabricated by electrospinning," *Nanoscale Research Letters*, vol. 4, no. 3, pp. 221–228, 2009.

[17] M. E. Rabanal, A. Várez, B. Levenfeld, and J. M. Torralba, "Magnetic properties of Mg-ferrite after milling process," *Journal of Materials Processing Technology*, vol. 143-144, no. 1, pp. 470–474, 2003.

[18] F. M. H. Zarandi and K. Sadrnezhaad, "Thermomechanical study of combustion synthesized Ti-Ni shape memory alloy," *Materials and Manufacturing Processes*, vol. 12, no. 6, pp. 1093–1105, 1997.

[19] K. C. Patil, S. T. Aruna, and S. Ekambaram, "Combustion synthesis," *Current Opinion in Solid State and Materials Science*, vol. 2, no. 2, pp. 158–165, 1997.

[20] G. Xanthopoulou, "Catalytic properties of the SHS products," *Advances in Science and Technology*, vol. 63, pp. 287–296, 2010.

[21] J. J. Kingsley and K. C. Patil, "A novel combustion process for the synthesis of fine particle α-alumina and related oxide

materials," *Materials Letters*, vol. 6, no. 11-12, pp. 427–432, 1988.

[22] K. V. Rao and C. S. Sunandana, "Co_3O_4nanoparticles by chemical combustion: effect of fuel to oxidizer ratio on structure, microstructure and EPR," *Solid State Communications*, vol. 148, no. 1-2, pp. 32–37, 2008.

[23] T. K. Pathak, N. H. Vasoya, V. K. Lakhani, and K. B. Modi, "Structural and magnetic phase evolution study on needle-shaped nanoparticles of magnesium ferrite," *Ceramics International*, vol. 36, no. 1, pp. 275–281, 2010.

[24] S. K. Pradhan, S. Bid, M. Gateshki, and V. Petkov, "Microstructure characterization and cation distribution of nanocrystalline magnesium ferrite prepared by ball milling," *Materials Chemistry and Physics*, vol. 93, no. 1, pp. 224–230, 2005.

[25] S. Da Dalt, A. S. Takimi, V. C. Sousa, and C. P. Bergmann, "Magnetic and structural characterization of nanostructured $MgFe_2O_4$ synthesized by combustion reaction," *Particulate Science and Technology*, vol. 27, no. 6, pp. 519–527, 2009.

[26] V. Sachin. Bangale, D. R. Patil, and S. R. Bamane, "prepration and electrical properties of nanocrystalline $MgFe_2O_4$ oxide by combustion route," *Archives of Applied Science and Research*, vol. 3, no. 5, pp. 506–513, 2011.

[27] Y. L. Liu, Z. M. Liu, Y. Yang, H. F. Yang, G. L. Shen, and R. Q. Yu, "Simple synthesis of $MgFe_2O_4$ nanoparticles as gas sensing materials," *Sensors and Actuators B*, vol. 107, no. 2, pp. 600–604, 2005.

[28] A. A. Thant, S. Srimala, P. Kaung, M. Itoh, O. Radzali, and M. N. A. Fauzi, "Low temperature synthesis of $MgFe_2O_4$ soft ferrite nanocrystallites," *Journal of the Australian Ceramic Society*, vol. 46, no. 1, pp. 11–14, 2010.

[29] R. A. Candeia, M. A. F. Souza, M. I. B. Bernardi et al., "$MgFe_2O_4$ pigment obtained at low temperature," *Materials Research Bulletin*, vol. 41, no. 1, pp. 183–190, 2006.

[30] V. M. Khot, A. B. Salunkhe, M. R. Phadatare, and S. H. Pawar, "Formation, microstructure and magnetic properties of nanocrystalline $MgFe_2O_4$," *Materials Chemistry and Physics*, vol. 132, no. 2-3, pp. 782–787, 2012.

[31] S. Verma, P. A. Joy, Y. B. Khollam, H. S. Potdar, and S. B. Deshpande, "Synthesis of nanosized $MgFe_2O_4$ powders by microwave hydrothermal method," *Materials Letters*, vol. 58, no. 6, pp. 1092–1095, 2004.

[32] B. D. Cullity, *Elements of X-Ray Diffraction?* Addison- Wesly Publishing, Notre Dame, Indiana, 3rd edition, 1976.

[33] P. Kameli, H. Salamati, and A. Aezami, "Effect of particle size on the structural and magnetic properties of $la_{0.8}Sr_{0.2}MnO_3$," *Journal of Applied Physics*, vol. 100, no. 5, Article ID 053914, 4 pages, 2006.

[34] T. K. Pathak, J. J. U. Buch, U. N. Trivedi, H. H. Joshi, and K. B. Modi, "Infrared spectroscopy and elastic properties of nanocrystalline Mg-Mn ferrites prepared by Co-precipitation," *Journal of Nanoscience and Nanotechnology*, vol. 8, no. 8, pp. 4181–4187, 2008.

[35] K. Parekh, R. V. Upadhyay, L. Belova, and K. V. Rao, "Ternary monodispersed $Mn_{0.5}Zn_{0.5}Fe_2O_4$ ferrite nanoparticles: preparation and magnetic characterization," *Nanotechnology*, vol. 17, no. 24, pp. 5970–5975, 2006.

[36] M. Sivakumar, T. Takami, H. Ikuta et al., "Fabrication of zinc ferrite nanocrystals by sonochemical emulsification and evaporation: observation of magnetization and its relaxation at low temperature," *Journal of Physical Chemistry B*, vol. 110, no. 31, pp. 15234–15243, 2006.

[37] R. D. Waldron, "Infrared spectra of ferrites," *Physical Review*, vol. 99, no. 6, pp. 1727–1735, 1955.